

## Crevasse and rift detection in Antarctica from TerraSAR-X satellite imagery



O.J. Marsh<sup>a,\*</sup>, D. Price<sup>b,c</sup>, Z.R. Courville<sup>d</sup>, D. Floricioiu<sup>e</sup>

<sup>a</sup> British Antarctic Survey, Cambridge, UK

<sup>b</sup> Antarctica New Zealand, Christchurch, New Zealand

<sup>c</sup> Gateway Antarctica, University of Canterbury, Christchurch, New Zealand

<sup>d</sup> U.S. Army ERDC-Cold Regions Research & Engineering Laboratory, Hanover, NH, USA

<sup>e</sup> DLR, German Aerospace Center, Oberpfaffenhofen, Germany

### ARTICLE INFO

#### Keywords:

Ice shelf  
Shear zone  
Fracture  
Traverse  
Polarization  
Backscatter  
Brunt Ice Shelf  
McMurdo Shear Zone

### ABSTRACT

Surface crevasses covered by snow bridges can be mapped remotely on ice sheets and glaciers using active microwave synthetic aperture radar. They are highlighted against the surrounding snow due to increased scattering from the side-walls and base of snow bridges and usually appear as linear features. The contrast between crevasses and crevasse-free regions depends on the design of the sensor, the image acquisition parameters and the properties of the snow. Here we quantify how crevassed regions are represented at X-band for different polarizations, look directions and incidence angles, and discuss whether additional information about their physical properties can be gained from their radar signature. Snow bridge thicknesses and crevasse widths are measured on the ground in the McMurdo Shear Zone and Brunt Ice Shelf by ground-penetrating radar and excavation. TerraSAR-X is shown to reliably distinguish crevasse location, balancing penetration into the snow and horizontal resolution. We provide recommendations for radar imaging parameters that optimize the identification of individual crevasses and crevassed regions.

### 1. Introduction

Surface crevasses are widespread in Antarctica. They form in regions of high strain rate where extensional stress exceeds the fracture toughness of the ice. This occurs in shear zones at the margins of fast flowing outlet glaciers and ice streams, close to ice shelf fronts where ice is unconfined, or where there is a local change in basal topography causing along-flow changes in velocity (Colgan et al., 2016). Crevasses and rifts on ice shelves advect with ice flow and so can also occur well away from where they originally formed. Many crevasses do not show a surface expression (Nath and Vaughan, 2003) as they are masked by drifting snow which can form snow bridges several metres wide and of variable strength and thickness. The hidden nature of bridged crevasses makes them particularly hazardous for operations in Antarctica.

Ground-penetrating radar (GPR) is a valuable tool to image the subsurface for glaciological applications (Taurisano et al., 2006; Cook, 1956). It is used as a standard procedure by the US, UK and NZ Antarctic programs (amongst others) for identifying upcoming hazards during snowmobile and heavy vehicle traverses through glaciated terrain. The use of vehicle-mounted GPR requires constant monitoring during traverses and it is not possible to identify crevasses in this way without

physically approaching them, with an associated risk to personnel. Aircraft-mounted GPR can cover large regions in a safe way, but is costly. There is ongoing research into the use of unmanned vehicles for crevasse mapping (Lever et al., 2013; Arcone et al., 2016; Kaluzienski et al., 2019) but all these GPR-based techniques lack the ability to map large regions at high spatial density. In 2006, airborne investigations over snow covered crevasses were carried out close to McMurdo Station with MiniSAR at X-band (Sander and Bickel, 2007). These data showed the potential to detect crevasses in the presence of snow bridges and the influence of look direction on appearance. Further theoretical work shows that X-band should provide a suitable balance between spatial resolution and penetration depth (Brock, 2010), and crucially can operate from satellite.

Here we investigate the value of satellite-based radar systems for crevasse identification, with the benefit that bridged crevasses can be identified remotely prior to deployment into the field, and that surveys can be repeated as needed. Unlike visible wavelength sensors, microwave radar penetrates into the upper layers of the snow. This is a valuable tool for identifying hidden hazards on planned traverse routes as well as for mapping the orientation and extent of crevasse fields for glaciological research. Several suitable high-resolution radar satellites

\* Corresponding author.

E-mail address: [olrs@bas.ac.uk](mailto:olrs@bas.ac.uk) (O.J. Marsh).

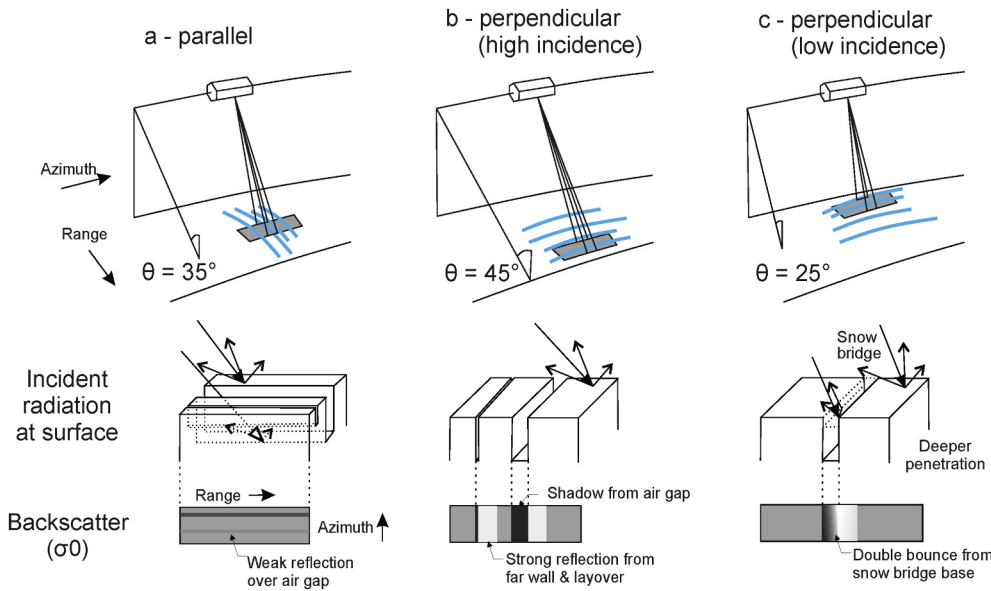


**Fig. 1.** Schematic representing the variation in imaged backscatter under different geometries and crevasse types. The three columns indicate differences in incidence angle and look direction. The top row is the satellite and crevasse geometry, the middle row is a diagrammatic representation of how incident radiation scatters due to crevasses of different width, and the bottom row an indication of the resulting backscatter intensity of the SAR image, where lighter shading indicates higher backscatter.

are currently in operation at microwave frequencies. The value of the imagery as a method to mark out rifts and crevasses depends on a range of factors including the satellite orbital characteristics; the sensor frequency and imaging mode; the properties of the crevasse or crevasse field; and the properties of the surrounding snow. All are discussed hereafter, with recommendations made for radar satellite surveys of crevassed regions.

## 2. Theoretical basis

Active microwave satellite radar systems emit pulsed radiation towards the Earth's surface and detect the proportion that is backscattered to the sensor. This value normalized over unit area is known as the backscatter coefficient ( $\sigma_0$ ). It is a function of the overall reflectance of the material and the bidirectional distribution of that reflected radiation. The reflectance is determined by the dielectric properties of the snow, while the distribution is related to the interface roughness.

At a randomly rough air/snow boundary a small part of the incident wave is reflected back into the air and one part is transmitted through the interface and propagates through the snow. The fraction of the incident radiation reflected at the air/snow interface can be approximated by the Fresnel power reflection coefficient  $\Gamma_{h,v}$  (1), although slightly reduced by diffuse scattering. The remaining radiation is transmitted into the snowpack  $\Gamma_{h,v} + \gamma_{h,v} = 1$ , where  $h$  and  $v$  are the horizontal and vertical polarization of the electromagnetic wave.

$\Gamma_{h,v}$  is a function of the electric permittivity of the medium ( $\epsilon = \epsilon' + \epsilon''i$ ), the polarization of the incident radiation (horizontal (h) or vertical (v)) and its incidence angle ( $\theta$ ):

$$\begin{aligned}\Gamma_h &= \left( \frac{\cos\theta - \sqrt{\epsilon - \sin^2\theta}}{\cos\theta + \sqrt{\epsilon - \sin^2\theta}} \right)^2 \\ \Gamma_v &= \left( \frac{\sqrt{\epsilon - \sin^2\theta} - e\cos\theta}{\sqrt{\epsilon - \sin^2\theta} + e\cos\theta} \right)^2\end{aligned}\quad (1)$$

At microwave frequencies, the relative permittivity of pure ice ( $\epsilon_i'$ ) is independent of temperature and wavelength (Ulaby, 1982). The permittivity of dry snow, a homogenous mixture of air and ice ( $\epsilon_{ds}'$ ) is therefore only proportional to its density and is roughly in the range 1.4–2.0. In consequence, significant transmission takes place across the air/snow boundary for a wide range of incidence angles at both linear polarisations.

The imaginary part of the permittivity ( $\epsilon''$ ) which defines absorption is several degrees of magnitude smaller than the real part for dry snow but absorption losses increase significantly when liquid water content increases above a fraction of 1% volume. In order to approximate the penetration depth of the SAR signal in the snow pack we use a volume absorption coefficient of a homogeneous medium ( $\gamma_a$ ) and a volume scattering coefficient based on the classical radiative transfer theory assuming independently randomly distributed scatterers and no correlation between the fields scattered by the different particles ( $\gamma_s$ ):

$$\gamma_a = \frac{4\pi f}{c} \left\{ \frac{\epsilon'_{ds}}{2} \left[ \sqrt{1 + \left( \frac{\epsilon''_{ds}}{\epsilon'_{ds}} \right)^2} - 1 \right] \right\}^{\frac{1}{2}} \quad (2)$$

$$\gamma_s = 32 \left( \frac{\pi f}{c} \right)^4 \frac{\rho_s r^3}{\rho_i} \left| \frac{\epsilon_i - 1}{\epsilon_i + 2} \right|^2 \quad (3)$$

where  $r$  is the radius of snow grains,  $f$  is frequency,  $c$  is the speed of light and  $\rho_i$  and  $\rho_s$  are the densities of ice and snow, respectively (Davis and Moore, 1993). The two way penetration depth of a wave travelling off-nadir ( $d_p$ ) at the refraction angle ( $\theta'$ ) is inversely proportional to the total extinction ( $\gamma_a + \gamma_s$ ):

$$d_p = \frac{\cos\theta'}{2(\gamma_a + \gamma_s)} \quad (4)$$

For dry fine grained snow the scattering coefficient is significantly lower than the absorption coefficient. While this approach makes assumptions of homogeneity within the medium, no multiple scattering and does not account for depth changes in crystal properties, density or water content, it illustrates how incidence angle, surface properties and water content influence overall backscatter (Rees, 2012):

$$\sigma_\theta^0 = \Gamma_{h,v}^2(\theta) \gamma_s d_p + \sigma_{surface}^0(\theta) \quad (5)$$

The two way penetration depth ( $d_p$ ) in eq. 4, approximates the phase centre of the backscattered return (Dall, 2007). It is an important property in understanding the surface being imaged in radar altimetry and the accuracy of synthetic aperture radar systems for DEM creation and velocity mapping (Rignot et al., 2001). For our application, the penetration depth corresponds to the approximate thickness of snow bridges after which crevasses may become invisible in a radar image. A penetration depth of several metres or higher is desirable to image shallow subsurface crevasses. Rott et al. (1993) estimated a two-way

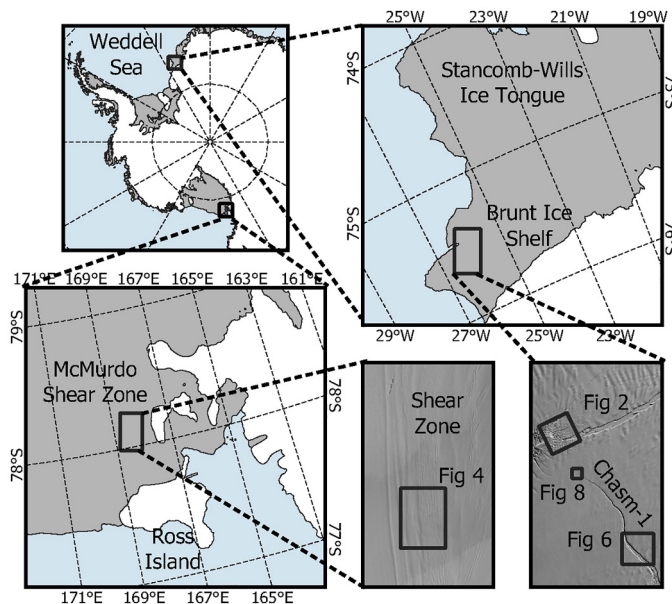


**Fig. 2.** Location of field validation sites.

penetration depth of 4.05 m for dry snow at 10 GHz which is in agreement with data collected in the interior of Greenland (Rizzoli et al., 2017). Independently, the average penetration depth of X-band radar from TerraSAR-X has been calculated as part of TanDEM-X validation and uncertainty estimation as between 3 and 7 m over dry snow (Zhao and Floricioiu, 2017). Lower frequencies (C-band and L-band) would be expected to penetrate further but with some loss of resolution.

In addition to the volume scattering and surface scattering from the air/snow interface, if a snow bridge exists but its thickness is less than the penetration depth there is a second snow-air interface at the base of the snow bridge. The additional material transition provides an additional surface that can enhance the backscatter. The structure of crystals within the snow bridge itself, modified by the cool microclimate below, for example through the formation of hoar (Colgan et al., 2016), may also provide additional scattering. Where there is no snow bridge, there is no horizontal surface from which to scatter and so a large open crevasse may appear as a comparatively dark region in a radar image. Both bridged and unbridged crevasses have a vertical surface at the

crevasse side wall providing an additional scattering surface. In the case of a bridged crevasse, the side wall and base of the snow bridge may interact further to a limited extent through double bounce scattering (Fig. 1). As crevasses and rifts generally form in a single direction relative to the stress field, they often appear as linear features with higher backscatter but may be cross-cutting in multiple directions where the fracture history is complex.

### 3. Study regions

We identify two areas for detailed study and field validation: the Brunt Ice Shelf where a heavily monitored rift is repeatedly surveyed (De Rydt et al., 2019) and the McMurdo Shear Zone which forms part of the South Pole Traverse Route and where crevasse bridges are opened with explosives, presenting a unique opportunity for visual inspection (Kaluzienski et al., 2019) (Fig. 2). The rift known as Chasm-1 on the Brunt Ice Shelf tapers from several hundred metres wide to a narrow tip and passes through ice of varying properties. It extended by several

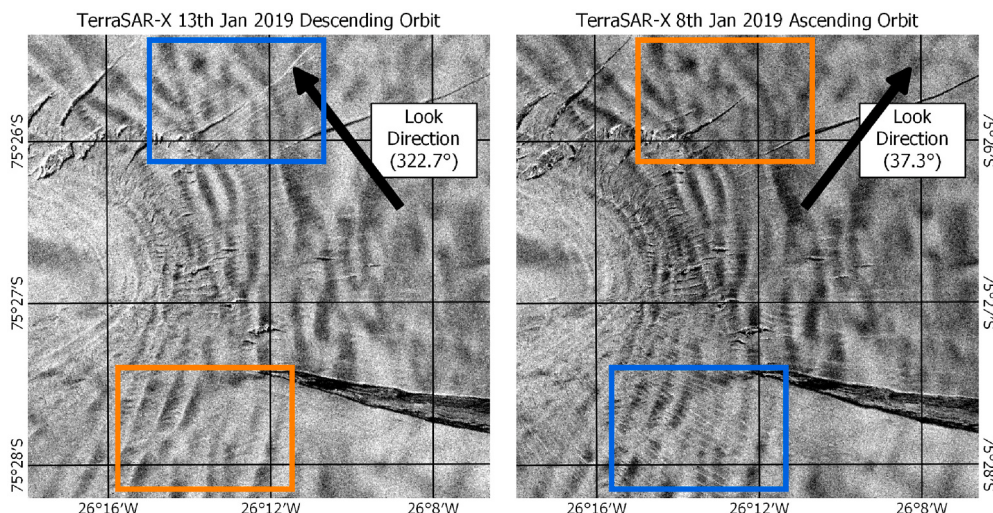


**Fig. 3.** Crevasse visibility is influenced by orientation relative to look direction as shown over the McDonald Ice Ripples. The crevasses in the blue boxes are largely perpendicular to the look direction, while the crevasses in the orange boxes are largely parallel to look direction. Images were acquired a few days apart during January 2019 with the same incidence angle ( $42.9^\circ$ ) and polarization (HH).

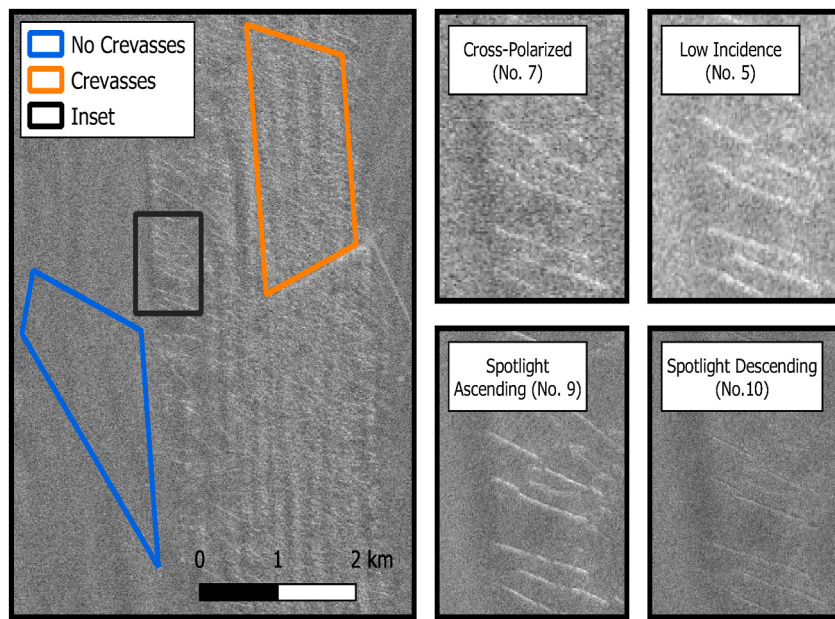


**Fig. 4.** Regions used for backscatter analysis in the McMurdo Shear Zone. Insets (black box) show how linear features bridged by several metres of snow are represented for selected imaging geometries. Image numbers and properties are listed in Table 1.

kilometres during 2019 and widened significantly in situ. The rift walls are flat and smooth at the centimetre-scale. It is sometimes bridged by snow. Nearby, a series of radial rifts in a region known as the McDonald Ice Ripples occupy a full  $90^\circ$  in orientation, allowing us to study the influence of look direction on crevasse visibility. The McMurdo Shear Zone is a narrow band of complex and sometimes cross cutting crevasses formed from the movement of the fast-flowing Ross Ice Shelf past the more slowly flowing McMurdo Ice Shelf. Snow bridges vary in width and thickness but are well-studied due to the logistical requirement of frequent traverses through this region. This shear zone is fairly representative of the type of non-uniform crevasse field that would be found in shear zones near outlet glaciers and fast flowing regions elsewhere in Antarctica.

#### 4. Optimal imaging characteristics

Here we describe how crevasses appear under a range of different imaging geometries. Most of this work is conducted with TerraSAR-X HH polarized stripmap imagery, although other satellites and other polarizations are also discussed. TerraSAR-X spotlight mode is also used, which applies phased array beam steering in azimuth direction to increase the illumination time of a small region, also increasing the spatial resolution. HH is the default polarization for TerraSAR-X and in the particular case of crevasses where a double bounce scattering mechanism may occur, it appears to have the advantage of higher backscattering than VV polarization, reducing the effect of random noise and leading to better coherence between images.

##### 4.1. Crevasse orientation and look direction

The backscatter signal from a crevasse depends very strongly on its orientation (Brock, 2010). Crevasses which are orientated perpendicular to the satellite look direction produce a high backscatter contrast relative to the surrounding snow, while crevasses that are parallel result in more forward scattering and are difficult to distinguish. As the radar signal reflects from the side walls of the crevasse, a parallel crevasse does not necessarily provide a strong reflecting surface. Fig. 3 shows a series of radial crevasses around an ice rise orientated between  $45^\circ$  in the north and  $135^\circ$  in the south. Bridged crevasses that are orientated at

$\pm 45^\circ$  oblique to look direction are still visible, although the contrast decreases as this increases towards parallel. In general two perpendicular directions should be able to highlight all crevasses. Larger unbridged crevasses and rifts appear as dark, low-backscatter features. There is no backscatter from the air gap within the crevasse. In these larger features, a high backscatter line can still be seen at the farthest edge, representing radar foreshortening due to the vertical face. When the crevasse width exceeds the image ground resolution, features become more easily distinguishable in images at sub-optimal look directions (Fig. 3).

##### 4.2. Incidence angle

Incidence angle ( $\theta$ ) determines both the penetration depth and the extent of foreshortening and shadowing at the crevasse walls. To compare the variation in rift visibility in a more quantitative way, we have statistically analyzed two regions of the McMurdo Shear Zone. The blue outlined region in Fig. 4 contains no crevasses, while the orange region is heavily crevassed. These two regions should produce different backscatter histograms. In the crevasse-free zone, there is a strong variation in overall backscatter with incidence angle (Fig. 5 and Table 1). The steeper the incidence angle, the higher the backscatter. Look direction has little influence in the crevasse-free region. Crevasse visibility is dependent on a high contrast between crevasses and crevasse-free regions, so a large difference in mean backscatter from the two regions is desirable and indicates that the crevasses are ‘more visible’. It can be seen that the lower the incidence angle the higher the contrast between the crevassed and crevasse-free regions.

##### 4.3. Polarization

Layering occurs in the snowpack due to density differences associated with individual accumulation or wind events. Vertically polarized microwave radiation is preferentially transmitted due to its lower reflection coefficient, while horizontally polarized radiation is reflected (West et al., 1996). The difference in penetration into the snowpack between vertically polarized and horizontally polarized incident radiation also depends strongly on the incidence angle (Leinss et al., 2014). Our investigations into polarization are spread over different time

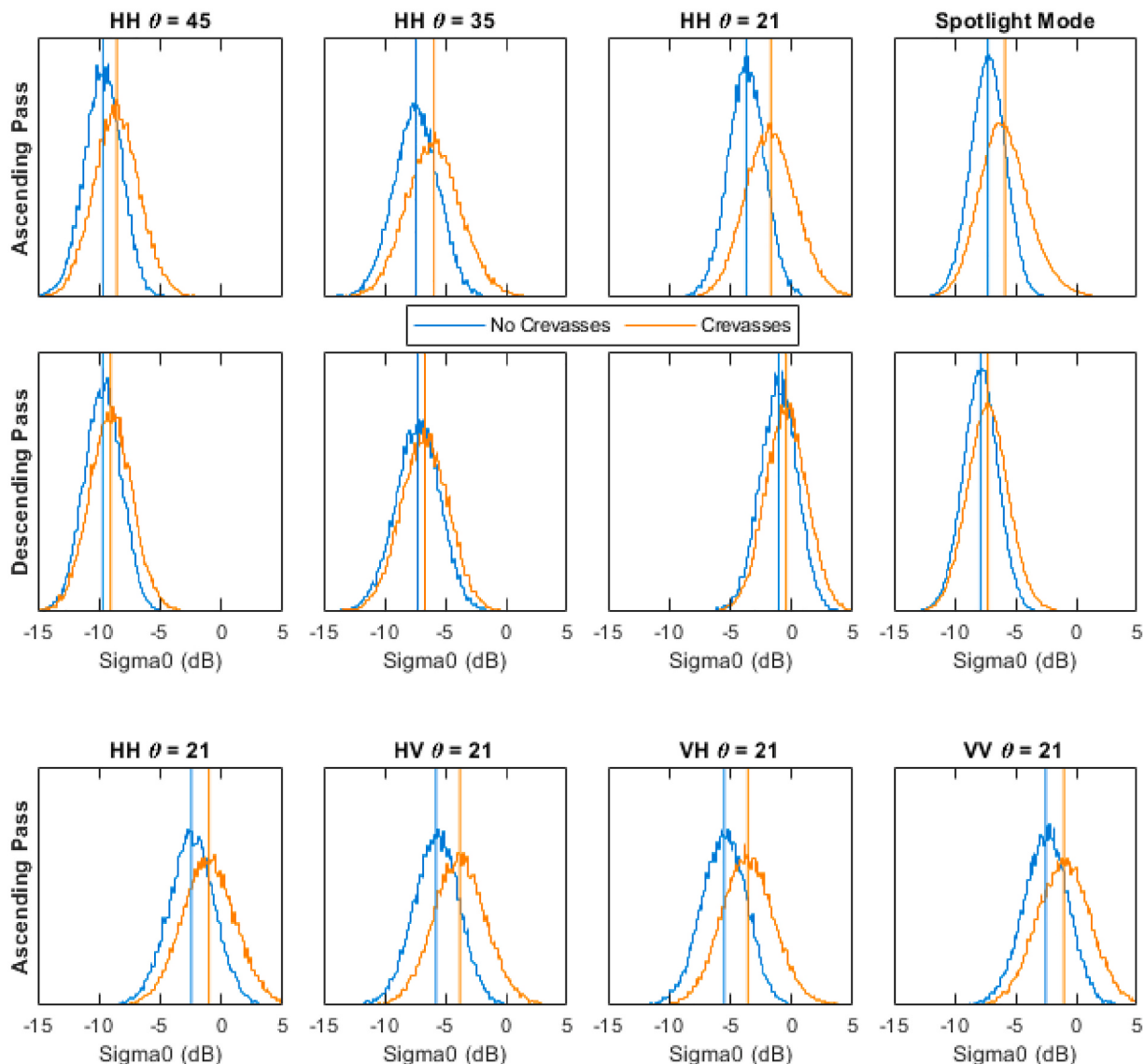


**Fig. 5.** a. Backscatter probability distributions in crevassed and non-crevassed regions of the McMurdo Shear Zone for different TerraSAR-X incidence angles and look directions. The extent of the blue and orange regions are shown in Fig. 4. Images were acquired between 12<sup>th</sup> and 22<sup>nd</sup> October 2019. b: Backscatter probability distributions under different polarizations for the same region as Fig. 2. Images were acquired between 10<sup>th</sup> and 21<sup>st</sup> April 2020. (For interpretation of the references to colour in this figure legend, the reader is referred to the web version of this article.)

periods but it is clear that overall backscatter is reduced in cross-polarized imagery. While the largest difference in contrast between crevasses and crevasse-free areas is in the HV polarized image (Fig. 5), the overall reduction in power of 3 to 8 dB (and resulting increase in noise) outweighs the benefits.

#### 4.4. Snow properties

Wet snow has a significantly higher absorption than dry snow. We see this effect during warm periods on the Brunt Ice Shelf. The presence of open rifts and crevasses themselves can impact the turbulent heat flux and lead to increased melt (Pfeffer and Bretherton, 1987). On the Brunt Ice Shelf ablation is increased on the down-wind side of rifts and backscatter is significantly reduced in these regions when temperature exceeds the melting point (Fig. 6). Alternating between melting and refreezing produces horizontally oriented crusts at the surface and vertically-oriented clusters of grains due to percolation. The large snow grains formed during the metamorphism are effective scatterers and the overall backscattering increases. This has the side effect of increasing

density and grain size contrasts in the upper layers and also increases the extinction rate, reducing the overall penetration depth and masking more deeply buried features. A sequence of images from one orbit at a constant incidence angle was acquired over the Brunt Ice Shelf between September 2018 and April 2020. A short warm period in December 2018 led to an immediate drop in backscatter followed by a sustained increase, while two more prolonged warm periods in December 2019 and January 2020 led to a more substantial increase in backscatter and reduction in the visibility of subsurface features (Fig. 7). This seasonal variation in backscatter and the influence on crevasse visibility is also seen in the McMurdo Shear Zone by comparing acquisition numbers 5 and 11 from Table 1 which have the same imaging characteristics in October 2019 and April 2020. Overall backscatter is higher in April but the contrast between crevassed areas and non-crevassed areas is reduced.

The fact that a large portion of the microwave radiation penetrates into the snowpack means the backscatter can be strongly affected by grain size, ice lenses and snow properties. Wind compaction and the formation of depth hoar change these properties spatially and over time.

**Table 1**

$\sigma_0$  values for the McMurdo Shear Zone under different TerraSAR-X imaging geometries. Images 1–10, were acquired between 12<sup>th</sup> and 22<sup>nd</sup> October 2019, while images 11–14 were acquired in between 10<sup>th</sup> and 21<sup>st</sup> April 2020. Bold values of  $\Delta$  indicate the rows with the highest backscatter contrast caused by crevassing.

No.	Name	Heading	$\theta(^{\circ})$	Pol	$\sigma_0(\text{dB})$		
					No Crevasse	Crevasse	$\Delta$
1	High $\theta$ (shallow)	284° A	44.6	HH	-9.69	-8.56	1.13
2		259° D	44.6	HH	-9.72	-9.05	0.67
3	Mod $\theta$	299° A	34.9	HH	-7.43	-5.94	1.49
4		242° D	35.9	HH	-7.29	-6.70	0.59
5	Low $\theta$ (steep)	310° A	21.4	HH	-3.70	-1.67	<b>2.03</b>
6		230° D	21.4	HH	-1.07	-0.45	0.62
7	Cross Polarized	299° A	34.9	HV	-12.98	-10.21	<b>2.77</b>
8		242° D	35.9	HV	-13.39	-11.84	1.55
9	Spotlight	300° A	32.5	HH	-7.26	-5.86	1.40
10		244° D	37.5	HH	-7.89	-7.27	0.62
11	Low $\theta$ , MultiPol	310° A	21.4	HH	-2.46	-1.03	1.43
12		310° A	21.4	HV	-5.75	-3.81	1.94
13		310° A	21.4	VV	-2.52	-1.02	1.50
14		310° A	21.4	VH	-5.53	-3.57	1.96

An accurate quantification of the relationship between snow properties and backscatter has useful applications for accumulation mapping (Dierking et al., 2012), but further discussion of the interaction of microwaves at the granular scales is beyond the scope of this study. While the absolute penetration depth, and therefore thickness of snow bridges that can be resolved, will change from area to area and over time, the most critical factor in the identification of crevasses appears to be the presence or absence of significant surface melting. Using satellite radar for crevasse detection will therefore fail in regions of Antarctica where temperatures regularly exceed 0 °C, particularly when images are acquired in mid-late summer. It is recommended that radar acquisitions for crevasse identification are scheduled outside the warmest months, when water content is low and higher penetration should lead to most clearly resolved sub-surface features.

#### 4.5. Frequency and spatial resolution

When considering the optimal frequency for imaging subsurface crevasses, there is a balance between penetration into the snow, horizontal resolution and the size of the coverage required. L-band radar can penetrate up to 100 m (Rignot et al., 2001), which is excessive for studying near surface features, while Ka and Ku band are likely to penetrate only between a few metres and a few centimetres (Slater et al.,

2019). There are several C-band (Sentinel-1 or Radarsat-2) and X-band (TerraSAR-X and CosmoSkyMed) systems currently in operation, which have a theoretical ability to observe sub-surface crevasses. Comparisons with C-band Radarsat-2 and Sentinel-1 suggest some finer detail is lost relative to TerraSAR-X due to lower resolution, particularly in comparison to the TerraSAR-X Spotlight mode. Modelling of radar interactions with crevasses also suggests that X-band is the optimal wavelength to images features at a depth of 4 m (Brock, 2010).

## 5. Ground validation

While being able to map crevasse location is a vital first step in understanding ground conditions, other characteristics such as width and snow bridge thickness determine the safety of travel in an area. Here we compare the observed patterns of crevasses seen with satellite radar imagery with ground observations and ground penetrating radar. We use the optimum imaging characteristics described above for mapping the features and determine whether additional characteristics of the crevasses (on top of just their location) can be determined by satellite alone.

### 5.1. Snow bridge thickness

In the McMurdo Shear Zone, snow bridge thicknesses vary from

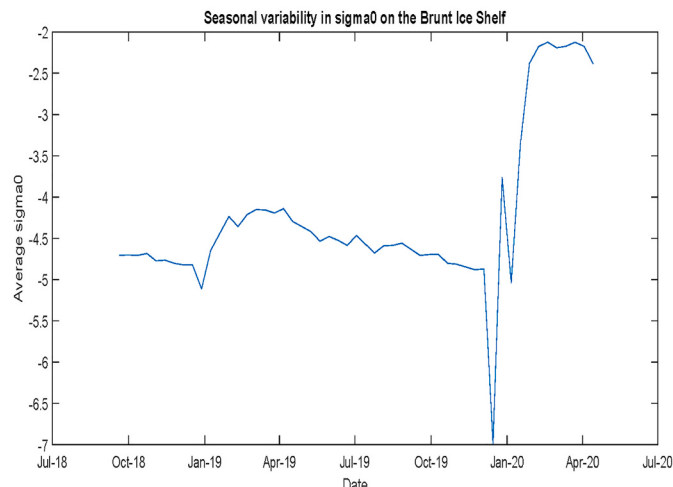


**Fig. 7.** Seasonal variability in average backscatter on the Brunt Ice Shelf shows a drop during melt events followed by an overall increase once new ice layers form, decreasing penetration and reducing crevasse visibility. All images in HH polarization with  $\theta = 42.9^{\circ}$ .

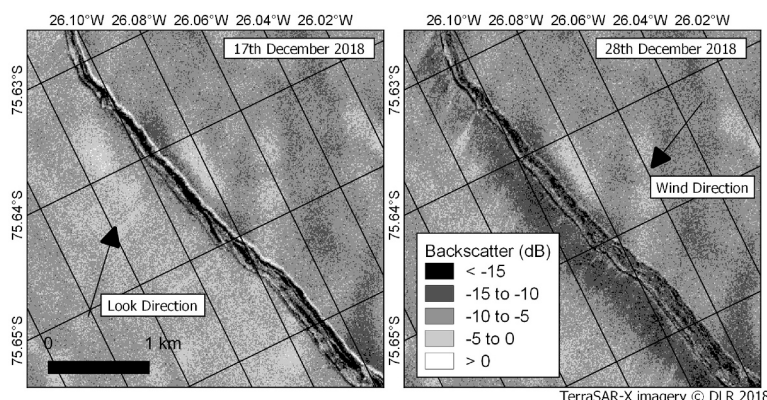


**Fig. 6.** Change in backscatter downwind of a rift on the Brunt Ice Shelf caused by turbulent heat flux associated with positive air temperatures.

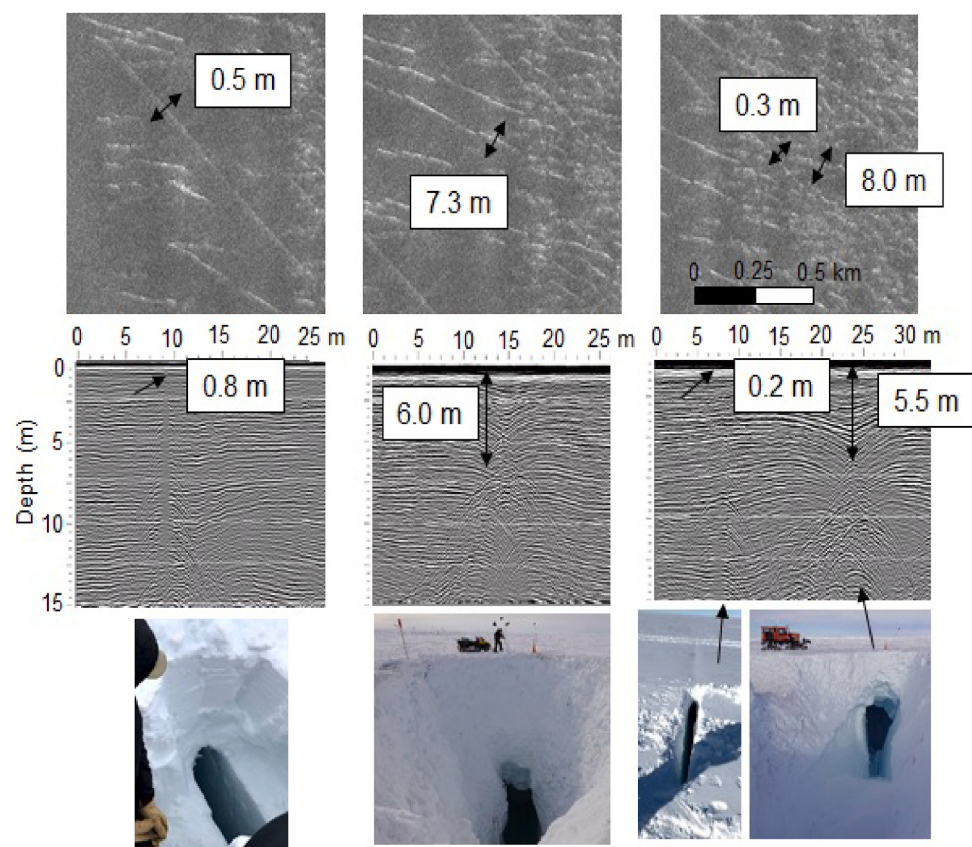


**Fig. 8.** Ground-penetrating radar data and ground observations in the McMurdo Shear Zone show that narrow, shallow crevasses have a similar brightness to wider crevasses at depth. All TerraSAR-X imagery is from image number 9 in Table 1 (Spotlight Ascending).

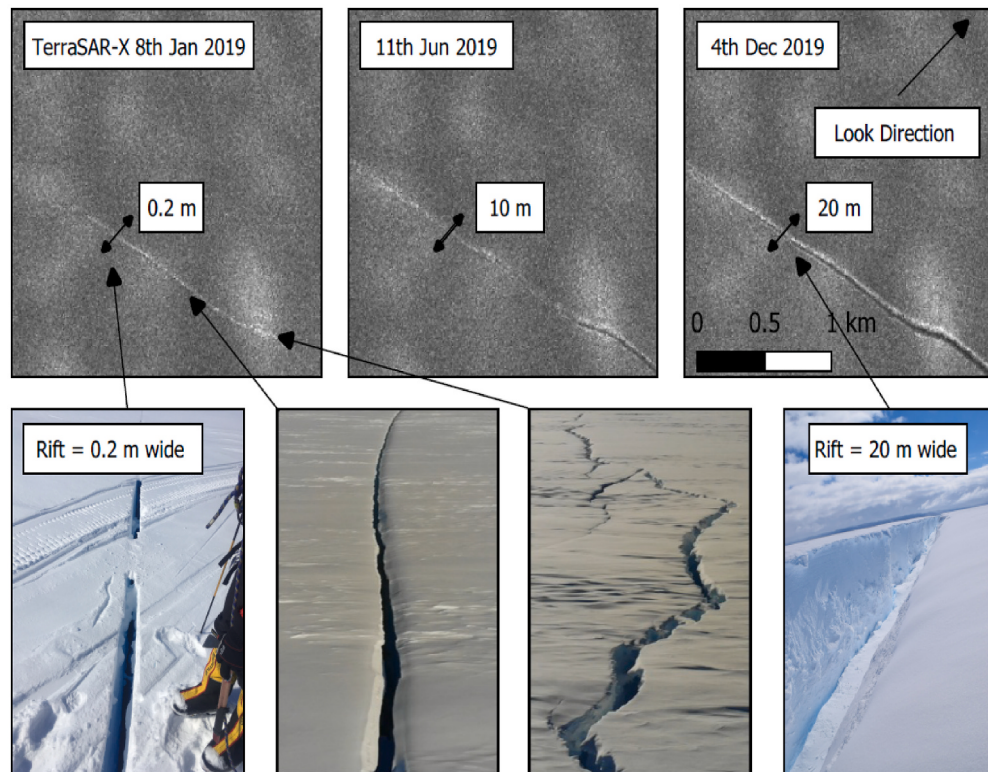


**Fig. 9.** Observations on the Brunt Ice Shelf of variable rift width for a constant imaging geometry. The photos show the surface impression of the rift at the same location, separated by one year of widening, while the aerial images show how crevasse geometry can modify the satellite representation of the reflection.

several metres to over 10 m. On the Brunt Ice Shelf some snow bridges are partially collapsed or sag in the middle, while other rifts are open at the surface. The difference in reflection for an open crevasse compared to a lightly bridged crevasse (e.g. 2 m thick) is significant and is evident where the same feature is bridged in some places and unbridged in others. Increasing the thickness of the snow bridge is expected to reduce the reflection from the crevasse as a lower proportion of incident radiation is received at the crevasse side-walls. Other factors including dipping layers and localized modification of the snow properties on the snow bridge may balance this out by enhancing the contrast in volume scattering (for instance due to circulation of cold air below the snow bridge and the formation of hoar). An approximately 6 m thick snow bridge covering a crevasse 8 m wide in the McMurdo Shear Zone appears brightly in the perpendicular (ascending) TSX imagery, despite being close to the theoretical limit of what should be visible with X-band radar (Fig. 8). As the character of the reflection does not change consistently with observed variations in snow bridge thickness it is not currently possible to provide useful quantitative data on bridge thickness. This is unlikely to become possible using this technique without additional information on snow properties.

## 5.2. Crevasse width

Ground penetrating radar and excavations show that width is particularly difficult to estimate from satellite radar data. Even using the high-resolution spotlight imagery, here multi-looked onto a 2 m grid, the relative brightness or width in pixels does not reflect the actual width of the crevasses. A rift only a few centimetres wide and open at the surface, shows a strikingly similar brightness profile to a rift 10 m wide or more (Fig. 9). TerraSAR-X stripmap mode with  $4 \times 4$  multi-looking, leads to a ground resolution of around 8 m but this resolution does not correlate with the horizontal scale of the features that can be seen. This is corroborated elsewhere in Antarctica where we have observed tide-cracks only a few centimetres wide that appear quite clearly in TerraSAR-X imagery. Only when a crevasse or rift exceeds several tens of metres and is open at the surface does the signature change as the air gap causes a decrease in backscatter parallel to the strong reflection from the crevasse wall.

While it is difficult to accurately estimate width, the identification of features significantly narrower than the spatial resolution is very valuable, and an additional benefit over low-resolution visible wavelength satellite imagery.

## 6. Conclusion

Crevasses can be detected in radar imagery even when they are significantly narrower than the horizontal resolution of the image, or are buried beneath several metres of snow. In several cases, features observed at depths of 10 m or more with ground penetrating radar could be identified from their satellite radar backscatter signature. This is a tool that can change how crevasse risk is managed and reduced in Antarctic field operations. It also provides a scientific method for mapping crevassed regions to infer information about fracture and ice properties. Here we have shown that while the value of this imagery is high, optimizing the imaging parameters is vital for correctly identifying features. The results are backed up by modelling electromagnetic wave interaction with snow (Brock, 2010).

Here we show that the most important factor which impacts our ability to observe sub-surface features is water fraction in the snowpack. This has a large impact on total absorption, dramatically reducing the backscatter and penetration through the snow. The development of ice layers following melt events also leads to inhomogeneities close to the surface which reduce the penetration and our ability to observe deeper features. The best time to acquire radar imagery for this application is therefore in the second half of austral winter (September / October).

Of most importance with regard to sensor characteristics is the look

direction, which needs to be as close to perpendicular to the features as possible. Two complimentary look directions at  $90^\circ$  from each other (e.g. from ascending and descending orbits) should be sufficient to capture all features where their orientation is unknown a priori. Images acquired with a low incidence angle are more likely to highlight sub-surface crevasses due to the steeper angle of penetration and less surface scattering. Our data also suggests that crevasses induce relatively higher scattering in cross-polarized images, although overall reduction in power in dual-polarized images means that this is generally at the expense of increased noise in crevasse-free areas. TerraSAR-X does not acquire cross-polarized imagery in its high-resolution Spotlight mode and the benefits from using cross-polarized StripMap imagery do not outweigh the benefits of the higher-resolution Spotlight data. More work can be done to quantify the influence of grain size and covariance of polarization and incidence angle, but we recommend high-resolution X-band satellite radar as a standard tool to identify crevasse locations in polar regions.

The linear nature of crevasses means that falsely identifying crevasses where there are none due to random noise is unlikely, although the satellite identification of a crevasse does not always indicate a danger for travel given that a feature only centimetres in width can show up in the imagery. There does remain a danger of false negatives (i.e. not identifying a present crevasse) due to high water content in the snow or recent melting in the area modifying the near-surface crystal structure. On the McMurdo Ice Shelf and Brunt Ice Shelf however, where crevasses are identified within a scene, we have not observed additional crevasses on the ground within that same scene which weren't also visible in the satellite imagery. While this is a positive outcome, additional ground observations from other areas would be needed before this technique could be relied on by itself for safety applications.

## Author contributions

OM & DP = Conceptualization; All authors = Data curation, Formal Analysis, Writing - review & editing; OM Writing - original draft.

## Declaration of Competing Interest

The authors declare that they have no known competing financial interests or personal relationships that could have appeared to influence the work reported in this paper.

## Acknowledgements

TerraSAR-X imagery was provided by DLR through project HYD3673. Fieldwork and logistics in the McMurdo Shear Zone was supported by the National Science Foundation Office of Polar Programs Antarctic Infrastructure and Logistics Section. We thank Nicholas Holzschuh and an anonymous reviewer for positive feedback that improved the manuscript.

## References

- Arcone, S.A., Lever, J.H., Ray, L.E., Walker, B.S., Hamilton, G., Kaluzienski, L., 2016. Ground-penetrating radar profiles of the mcmurdo shear zone, Antarctica, acquired with an unmanned rover: Interpretation of crevasses, fractures, and folds within firm and marine icegr profiles of the mcmurdo shear zone. *Geophysics* 81, WA21–WA34.
- Brock, B.C., 2010. On the Detection of Crevasses in Glacial Ice with Synthetic-Aperture Radar. Sandia Report. <https://doi.org/10.2172/989382>.
- Colgan, W., Rajaram, H., Abdalati, W., McCutchan, C., Mottram, R., Moussavi, M.S., Grigsby, S., 2016. Glacier crevasses: Observations, models, and mass balance implications. *Rev. Geophys.* 54, 119–161. <https://doi.org/10.1002/2015RG000504>.
- Cook, J.C., 1956. An electrical crevasse detector. *Geophysics* 21, 1055–1070. <https://doi.org/10.1190/1.1438300>.
- Dall, J., 2007. In-sar elevation bias caused by penetration into uniform volumes. *IEEE Trans. Geosci. Remote Sens.* 45, 2319–2324.
- Davis, C.H., Moore, R.K., 1993. A combined surface-and volume-scattering model for ice-sheet radar altimetry. *J. Glaciol.* 39, 675–686. <https://doi.org/10.3189/S002214300016579>.

- De Rydt, J., Gudmundsson, G.H., Nagler, T., Wuite, J., 2019. Calving cycle of the brunt ice shelf, Antarctica, driven by changes in ice shelf geometry. *Cryosphere* 13, 2771–2787. <https://doi.org/10.5194/tc-13-2771-2019>.
- Dierking, W., Linow, S., Rack, W., 2012. Toward a robust retrieval of snow accumulation over the antarctic ice sheet using satellite radar. *J. Geophys. Res. Atmos.* 117. <https://doi.org/10.1029/2011JD017227>.
- Kaluzienski, L., Koons, P., Enderlin, E., Hamilton, G., Courville, Z., Arcene, S., 2019. Crevasse initiation and history within the mcmurdo shear zone, Antarctica. *J. Glaciol.* 65, 989–999. <https://doi.org/10.1017/jog.2019.65>.
- Leinss, S., Parrella, G., Hajnsek, I., 2014. Snow height determination by polarimetric phase differences in x-band Sar data. *IEEE J. Select. Topics Appl. Earth Observ. Remote Sens.* 7, 3794–3810.
- Lever, J., Delaney, A., Ray, L., Trautmann, E., Barna, L., Burzynski, A., 2013. Autonomous gpr surveys using the polar rover. *J. Field Robot.* 30 <https://doi.org/10.1002/rob.21445>.
- Nath, P.C., Vaughan, D.G., 2003. Subsurface crevasse formation in glaciers and ice sheets. *J. Geophys. Res. Solid Earth* 108. <https://doi.org/10.1029/2001JB000453>. ECV 7–1–ECV 7–12.
- Pfeffer, W., Bretherton, C., 1987. The effect of crevasses on the solar heating of a glacier surface. *Phys. Basis Ice Sheet Modell.* 170.
- Rees, W., 2012. *Physical Principles of Remote Sensing*. Cambridge University Press.
- Rignot, E., Echelmeyer, K., Krabill, W., 2001. Penetration depth of interferometric synthetic-aperture radar signals in snow and ice. *Geophys. Res. Lett.* 28, 3501–3504. <https://doi.org/10.1029/2000GL012484>.
- Rizzoli, P., Martone, M., Rott, H., Moreira, A., 2017. Characterization of snow facies on the greenland ice sheet observed by tandem-x interferometric sar data. *Remote Sens.* 9. <https://doi.org/10.3390/rs9040315>.
- Rott, H., Sturm, K., Miller, H., 1993. Active and passive microwave signatures of antarctic firn by means of field measurements and satellite data. *Ann. Glaciol.* 17, 337–343. <https://doi.org/10.3189/S0260305500013070>.
- Sander, G.J., Bickel, D.L., 2007. Antarctica X-band Minisar Crevasse Detection Radar: Final Report. Sandia Report. <https://doi.org/10.2172/920457>.
- Slater, T., Shepherd, A., Mcmillan, M., Armitage, T.W.K., Otosaka, I., Arthern, R.J., 2019. Compensating changes in the penetration depth of pulse-limited radar altimetry over the Greenland ice sheet. *IEEE Trans. Geosci. Remote Sens.* 57, 9633–9642.
- Taurisano, A., Tronstad, S., Brandt, O., Kohler, J., 2006. On the use of ground penetrating radar for detecting and reducing crevasse-hazard in dronning maud land, Antarctica. *Cold Reg. Sci. Technol.* 45, 166–177.
- Ulaby, F.T., 1982. *Microwave Remote Sensing Active and Passive. Rader Remote Sensing and Surface Scattering and Emission Theory*.
- West, R.D., Winebrenner, D.P., Tsang, L., Rott, H., 1996. Microwave emission from density-stratified antarctic firn at 6 cm wavelength. *J. Glaciol.* 42, 63–76. <https://doi.org/10.3189/S0022143000030537>.
- Zhao, J., Floricioiu, D., 2017. The penetration effects on tandem-x elevation using the gnss and laser altimetry measurements in Antarctica. *ISPRS – Intern. Arch. Photogrammet. Remote Sens. Spat. Inform. Sci.* XLII-2 (W7), 1593–1600. <https://doi.org/10.5194/isprs-archives-XLII-2-W7-1593-2017>.